Journal of Electrochemistry

Volume 23
Issue 2 *Special Issue in Honor of Professor Zhaowu Tian on His 90th Birthday*

2017-04-28

Green Electrochemical Ozone Production via Water Splitting: Mechanism Studies

Gregory Gibson

Wenfeng Lin
Department of Chemical Engineering, Loughborough University, Loughborough, Leicestershire, LE11 3TU, UK;, w.lin@lboro.ac.uk

Recommended Citation
Gregory Gibson, Wenfeng Lin. Green Electrochemical Ozone Production via Water Splitting: Mechanism Studies[J]. *Journal of Electrochemistry*, 2017 , 23(2): 180-198.
DOI: 10.13208/j.electrochem.161252
Available at: https://jelectrochem.xmu.edu.cn/journal/vol23/iss2/8

DOI: 10.13208/j.electrochem.161252 **Artical ID**:1006-3471(2017)02-0180-19
Cite this: *J. Electrochem.* **2017**, *23*(2): 180-198 **Http**://electrochem.xmu.edu.cn

Green Electrochemical Ozone Production via Water Splitting: Mechanism Studies

Gregory Gibson[1,2], Wenfeng Lin[1*]
(1. *Department of Chemical Engineering, Loughborough University, Loughborough, Leicestershire,* LE11 3TU, *UK*;
2. *School of Chemistry and Chemical Engineering, Queen's University Belfast, Belfast,* BT9 5AG, *UK*)

Abstract: The green and energy-efficient water splitting reaction using electrocatalysis for O_3 formation provides a very attractive alternative to the conventional energy-intensive cold corona discharge (CCD) method. Among a large number of electrocatalysts explored for the electrochemical ozone production, β-PbO_2 and SnO_2-based catalysts have proven to be the most efficient ones at room temperature. In this study Density Functional Theory (DFT) calculations have been employed to investigate the possible mechanisms of ozone formation over these two types of catalysts. For both the β-PbO_2 and Ni/Sb-SnO_2 (nickel and antimony doped tin oxide) catalysts the (110) facet was found to be the most stable one. The possible water splitting mechanisms were modeled on both the β-PbO_2 (110) and Ni/Sb-SnO_2 (110) surfaces with particular attention given to the final two reaction steps, the formations of O_2 and O_3. For the β-PbO_2, the formation of O_3 was found to occur through an Eley-Rideal style mechanism as opposed to that on the Ni/Sb-SnO_2, the latter occurs through a Langmuir-Hinshelwood style interaction. Thermodynamic parameters such as the adsorption energies (E_{ads}), Gibbs free energies (ΔG) and activation energies (E_{act}) have also been obtained, compared and presented, with β-PbO_2 being modelled primarily as solid-liquid phases and Ni/Sb-SnO_2 modelled as gas phase. These DFT findings have provided the basis for a tool to design and develop new electrochemical ozone generation catalysts capable of higher current efficiencies.

Key words: ozone evolution reaction; water splitting; density functional theory; electrocatalysis; surface adsorption and reaction; lead oxide; nickel and antimony doped tin oxide

CLC Number: O646 **Document Code**: A

The ozone evolution reaction is a fundamental reaction used in water purification employing advanced oxidation processes with ozone (O_3) as the principal oxidant[1-5]. O_3 is the second strongest oxidant behind chlorine (oxidation potential of 2.07 V vs. SHE), with the advantage that it does not produce the same harmful halogenated by-products that chlorine does. Ozone is not only used in water treatment but has a prevalent role in healthcare[6-7], sterilization[8-9] and in chemical synthesis[10]. The current method employed industrially to produce ozone is through the use of a cold corona discharge (CCD) reactor[11-12]. The reactions can be seen below:

$$e + O_2 \rightarrow 2O^{\cdot} + e \quad (R1)$$

$$O^{\cdot} + O_2 + M \rightarrow O_3 + M^* \quad (R2)$$

$$O^{\cdot} + O_3 \rightarrow 2O_2 \quad (R3)$$

$$e + O_3 \rightarrow O_2 + O^* + e \quad (R4)$$

In this process a source of dry O_2 is passed through the reactor and reacts with an electron source causing the O_2 atoms to dissociate into two O atoms. These O atoms next interact with O_2 molecules that have not been dissociated previously forming O_3 as the product. Whilst a relatively simple process in principal, the O_3 formation current efficiencies are reported as low, with the efficiencies of 2 ~ 12%[11]. Not only this low efficiency, but also the O_3 formed is a gas, making it difficult to be directly applied for aqueous applications such as water treatment due to its difficulty to dissolve once a gas.

In more recent time, a different method has been investigated with the potential to replace this CCD technology. Through the use of electrochemistry/elec-

Received: 2017-03-02, Revised: 2017-04-06 *Corresponding author, Tel: 0044-(0)1509 222506, E-mail: w.lin@lboro.ac.uk

trocatalysis, the production of O_3 can be achieved with high current efficiencies. The major drawback of this process is the competition between O_2 and O_3 formations with thermodynamics suggesting the formation of O_2 is favoured:

$$O_3 + 6H^+ + 6e \rightarrow 3H_2O \quad E^0 = 1.51\ V \qquad (R5)$$

$$O_2 + 4H^+ + 4e \rightarrow 2H_2O \quad E^0 = 1.23\ V \qquad (R6)$$

As seen from the standard electrode potentials (E^0), the formation of O_2 occurs at a lower potential than that for O_3 and therefore will be favoured. In order to promote the formation of O_3, O_2 formation must be inhibited. This could be done through the following steps:

·Suitable catalyst material must be chosen.

·Material must be chemically and mechanically stable as a very high anodic potential is needed for O_3 formation and then the gas evolution.

·Material used must have a high overpotential for oxygen evolution and be resistant to anodic polarization.

·Additives that partially inhibit the formation of O_2 by blocking the selected active sites may be used.

In order to satisfy these outlined parameters, the careful selection of a catalyst material is required. The literature gives many examples of different systems tested. One of the earliest examples reported employed a platinum catalyst [13-15]. More recently, boron-doped diamond (BDD)[16-17], PbO_2[18-19] and Ni/Sb/SnO_2[20-24] catalysts have been preferred as the efficiency values were much greater at room temperature than that of platinum. Of these the β-PbO_2 and Ni/Sb-SnO_2 systems are well studied experimentally and the most efficient, therefore, our initial theoretical study will focus on these two catalysts.

1) Electrochemical Studies on PbO_2 Based Electrodes

In 1982, Foller and Tobias pioneered the study of PbO_2, with particular emphasis on β-PbO_2[18]. Although β-PbO_2 was a superior catalyst in comparison to SnO_2, platinum and DSA (Dimensionally Stable Anode), it did have some disadvantages associated with it and this must be evaluated:

·Lead is toxic. This is problematic especially when considered for a water treatment application-where leaching could occur.

·Lead has a short lifetime. The high rates of lead dissolution at high potential have been noted in some cases.

·Lead has a largecurrent efficiency at low temperature with high energy penalty. Although at room temperature the current efficiency is considerably good (2 ~ 12%), however, to achieve larger current efficiency much lower temperatures are needed which incurs a high energy penalty.

In order to compete with CCD reactor technology which does not boast high efficiencies (2 ~ 12% by volume)[11] but does have a relatively long lifetime, the β-PbO_2 anodes can have moderate efficiencies but the anode lifetime must be improved. In 2012, Velichenko et al[25]. focused on overcoming the short lifetimes associated with lead oxide anodes. Through the process of electrodeposition, various oxides such as TiO_2 and ZrO_2 were added forming composite materials based on lead oxide. The addition of these oxides was said to have a pronounced effect on the lead oxide structure. After carrying out accelerated life time testing (ALT) it was found that by addition of these oxides and subsequent formation of the composite materials, the lifetime of the anodes increased. At a current density of 200 mA·cm^{-2} and 5wt% of TiO_2, the service life increased from 105 h to 207 h at the same operating conditions. This shows a two-fold increase in service life. The same increase in lifetime was reported for the ZrO_2 case. In 2014, Yao et al.[26] followed on the work carried out by Velichenko on composite lead oxide materials. The preparations of the anodes differ, as Velichenko used direct electrodeposition, whereas Yao used pulse electrodeposition. By using pulse deposition the Tan group[27] showed that PbO_2 possessed a stronger oxidation sta bility compared with direct deposition. ALT was again carried out to investigate the stability of the anode with the PbO_2-ZrO_2 composite electrode having a lifetime 4 times longer than PbO_2.

In 1998 and 2001, Amadelli and Velichenko[28-29] carried out studies on the influence of cations as

dopants. Although many cations have been tested in the past, iron and cobalt have shown the most promising results. The electrodeposition of PbO_2 in the presences of Fe(III) and Co(II) produces a doped material that is stable and has a high electrocatalytic activity for O_3 generation. After running experiments in 1 mol·L^{-1} H_2SO_4, the O_3 current efficiencies increased from less than 10% using PbO_2 to 20% using Fe-PbO_2 and 12% using Co-PbO_2. Not only does the doping improves current efficiency values, but provides electrode stability against corrosion, especially in the case of cobalt.

More recently Da Silva et al.[30] continued the initial work by Amadelli and Velichenko, choosing to focus on Fe-PbO_2 as opposed to the cobalt option, as this showed the highest performance between the two. Another study carried out by Rosestolato et al.[31] reports Fe doped anodes showing resistance to corrosion at high anodic potentials, hereby extending the lifetime by decreasing amorphisation of the electrocatalyst. The magnitude to which they increase depends on the individual characteristics such as the level of doping and the electrolyte employed. This is important as the stability of β-PbO_2 electrodes was one of the major problems found in Foller's research. The potential environmental aspect regarding the leaching of lead into the water has also been addressed using a solid polymer electrolyte (SPE) such as Nafion 117[30]. This SPE inhibits the solubilisation of Pb^{4+} ions and results in reduced leaching into wastewater.

Electrochemical ozone production (EOP) has substantially progressed since the initial work by Foller and Tobias, and the majority of the problems encountered have since been addressed by other groups. Although Foller et al. could generate ozone with current efficiency values of around 10%, the leaching of Pb^{4+} ions and short anode lifetime presented major problems. The leaching was by passed by the Da silva and Velichenko groups that employed a SPE, preventing the solubilisation of Pb^{4+} ions and so preventing leaching. The issue with short anode lifetime was tackled by the Velichenko and Yao groups, through doping of Fe and Co, and the formation of composite oxides PbO_2-ZrO_2 and PbO_2-TiO_2.

2) Electrochemical Studies on SnO_2-Based Electrodes

In 2004 Cheng and co-workers[32] reported a new SnO_2 system doped with Sb. Dissolved O_3 was produced from the anode in a UV cell containing 3 mL of 0.1 mol·L^{-1} $HClO_4$. The Sb-doped SnO_2 electrode was the working electrode that was placed at the bottom of the cell. A 0.8 cm^2 platinum electrode was used as the counter electrode in the upper regions of the cell close to the air. A reference electrode (Ag/AgCl) was placed next to the Sb-doped SnO_2. At 2.5 V (vs. Ag/AgCl) a constant potential was applied to the working electrode at room temperature. The concentration of dissolved O_3 was monitored by *in situ* UV spectroscopy at 258 nm with CE values reported to be ~15%. According to Cheng, efficiency values should be higher than quoted as some O_3 was released in the gaseous phase and therefore not accounted for in the efficiency calculations. This was confirmed by the distinct odour that O_3 gave off.

It was later found by Wang and co-workers[22] that the addition of a second dopant to the Sb-SnO_2 system had an effect on the overall performance. The second dopant used was a small amount of nickel. The anode was prepared by doping titanium mesh with nickel, antimony and tin-oxide and pyrolysed at 500 ℃. The dip-coating and pyrolysis process were repeated seven times. It was found that the best atomic ratio for these three elements was 1000:16:2 mmol·L^{-1} of Sn:Sb:Ni in the precursor solution. The addition of the nickel dopant caused an increase in O_3 generation efficiency to 32.5% at a potential of 2.2 V (vs. Ag/Ag Cl). It should be noted that 0.1 mol·L^{-1} H_2SO_4 was used as the electrolyte in this case. It was clear from the results that the nickel was causing the enhancement in the overall efficiencies; however no reason was given to explain the nickel effect.

Basiriparsa and Abbasi[20] presented an explanation to the effect that nickel had on increased current efficiencies. As nickel(III) has a lower valence than tin (IV) andmay act as an electron acceptor, which is capable of introducing positively charged holes in the

valence band by accepting electrons from the bulk. The electrons that are donated by antimony(V) and oxygen vacancies could be well compensated with the holes created by nickel(III), leaving the nickel site negatively charged. The negative charge around the nickel site would help to decrease the oxygen adsorption (hence inhibit oxygen evolution reaction). Therefore, after donating electrons, the positively charged antimony(V) sites could be considered Lewis acid sites, in which water was oxidized to OH· free radicals and O_2 would hereby form quickly. The O_2 formed on the antimony(V) site could then be transferred and adsorbed onto the nickel surface as an intermediate. The adsorbed O_2 reacted further with the OH· to form HO_3· radical that underwent a quick deprotonation forming O_3.

Further significant work was carried out by the Christensen and Lin group[23] following the procedure employed by Wanget al. but employing a larger anode surface area, a remarkable high current efficiency of 50% was achieved at a cell voltage of 2.7 V. The Ni/Sb-SnO_2 catalysts supported on Ti meshes underwent the dip-coating process for 20 times, with an optimal molar ratio of 3:8:500 for the Ni:Sb:Sn in the precursor solution. The counter electrode was a (5 × 5 cm) platinised titanium mesh. Rather than using a small UV cell (containing 3 mL of 0.1 mol·L^{-1} $HClO_4$) as seen before, this study utilised a large 200 cm^3 cell employing Nafion 117 proton exchange membrane (PEM) to separate anode and cathode in each half of the cell containing an aqueous 0. 5 mol·L^{-1} H_2SO_4 solution. An impressive low running cost, with the electricity usage of only 18 kWh per kg of ozone production, was achieved at room temperature. Furthermore, this system also produces hydrogen at the cathode which can be used as a fuel to feed in a fuel cell to generate electricity, which in turn can be used to offset the electricity cost in the ozone generation.

Concerning the water splitting mechanism for O_3 production, although discussed by various groups as to the accepted mechanism, there are no literature examples (other than our group) that have investigated the mechanism through the use of density functional theory (DFT) calculations[33-34]. Considering this, the β-PbO_2 and Ni/Sb-SnO_2 systems were initially chosen to study how the mechanism behaved. In fact β-PbO_2 was one of the first examples of a room temperature electrochemical ozone generation system that showed a greater efficiency than that of the CCD method, and the Ni/Sb-SnO_2 system is the best one in terms of current efficiency. In studying and comparing these two systems it was found that whilst the general mechanism on each catalyst surface could be the same, the surface reactions were found to occur through different modes of adsorption, not to mention the difference in O_2 and O_3 stabilities, and the activation energies for each reaction.

1 Theoretical Methods

1.1 Density Functional Theory

All density function theory (DFT) calculations were carried out with a periodic slab model using the Vienna Ab-initio simulation programme (VASP)[35-37]. A combination of the Generalised Gradient Approximation (GGA) and Perdew-Burke-Ernzernof (PBE) exchange correlation functional was applied[38]. The Projector Augmented Wave (PAW) method[39-40] was utilized to describe the electron-ion interactions, and the plane wave basis expansion cut-off was set to 500 eV. All adsorption energies where optimized using the force-based conjugate gradient algorithm, whereas the transition states (TS's) were located using the constrained minimization technique[41-43].

In the modelling of both the β-PbO_2 and Ni/Sb-SnO_2 surfaces, a stable facet for each must be determined. Four low index facets, the 100, 110, 111 and 211 arrangements were tested, and in both cases, it was the 110 facet that was deemed most stable. This is analogous to what was seen by Batzill et al.[44] for SnO_2 which is structurally the same as with β-PbO_2. Both surfaces where modelled as a(2 × 2) unit cell with various surface coverages tested (0. 25 ~ 1 ML). The two-dimensional Brillouin integrations for each were sampled using k-points for the(2 × 2) unit cell using a 3 × 3 × 1 Monkhorst-Pack grid. A four layer slab was employed with the lower two layers fixed and the upper two layers relaxed. Slab separation was

provided normal to the surface by employing a 1.5 nm vacuum region.

Unlike the β-PbO_2 which only has one metal component, the Ni/Sb-SnO_2 surface is made up of three components, the tin, antimony and nickel, and so additional work is required. The SnO_2 (Figure 1A) was first doped with antimony and next the Sb-SnO_2 surface was further doped with nickel. Of the four possible tin atoms on the surface each was replaced with an antimony atom, and then optimized to determine its preferred orientation (Figure 1B). This was repeated for the Ni/Sb-SnO_2 (Figure1C), with each of the remaining three tin atoms replaced with a nickel atom and again geometry optimization calculations were run with the lower two layers fixed and the upper two layers relaxed. The slab separation would remain at 1.5 nm throughout. All calculations for β-PbO_2, SnO_2, Sb-SnO_2 and Ni/Sb-SnO_2 were performed as spin-open.

With regards to the Ni/Sb-SnO_2 surface, the presence of a surface vacancy was also considered. It is a common phenomenon when testing these catalysts using experimental techniques that surface vacancies were detected. For this study an oxygen vacancy at the bridging site was introduced, as this is said to increase the activity at this site by increasing the Lewis acidity.

1.2 Surface Adsorption Calculations

The adsorption energy (E_{ads}) of the system was calculated using Equation 1:

$$E_{ads} = E_{adsorbate\ on\ surface} - E_{surface} - E_{gas} \quad \text{(E1)}$$

where $E_{adsorbate\ on\ surface}$ is the energy of the adsorbate and the surface, $E_{surface}$ is the energy of the clean surface and E_{gasis} the energy of the corresponding adsorbing species in the gas phase. Equation 1 shows that the more negative the adsorption energy is, the greater the adsorption to the surface. Each term in Equation 1 must correspond to the same surface coverage, whether this is a pure metal or metal oxide.

2 Results and Discussion

Experimentally, the method for producing O_3 electrochemically has been well studied. However, the exact mechanism by which O_3 formation precedes remains unsolved. It is commonly accepted that the mechanism proceeds via a four-step mechanism involving the splitting of H_2O to form O_3[17-18, 45-48]:

$$H_2O \rightarrow OH^{\bullet}(ads) + H^+ + e \quad \text{(R7)}$$

$$OH^{\bullet}(ads) \rightarrow O^{\bullet}(ads) + H^+ + e \quad \text{(R8)}$$

$$2O^{\bullet}(ads) \rightarrow O_2(ads) \rightarrow O_2 \quad \text{(R9)}$$

$$O_2(ads) + O^{\bullet}(ads) \rightarrow O_3(ads) \rightarrow O_3 \quad \text{(R10)}$$

Although each of the four steps is investigated indi vidually, it is Reactions 9 and 10 that are the most in teresting thermodynamically and therefore the majority of the results presented in detail will be concerning these two steps.

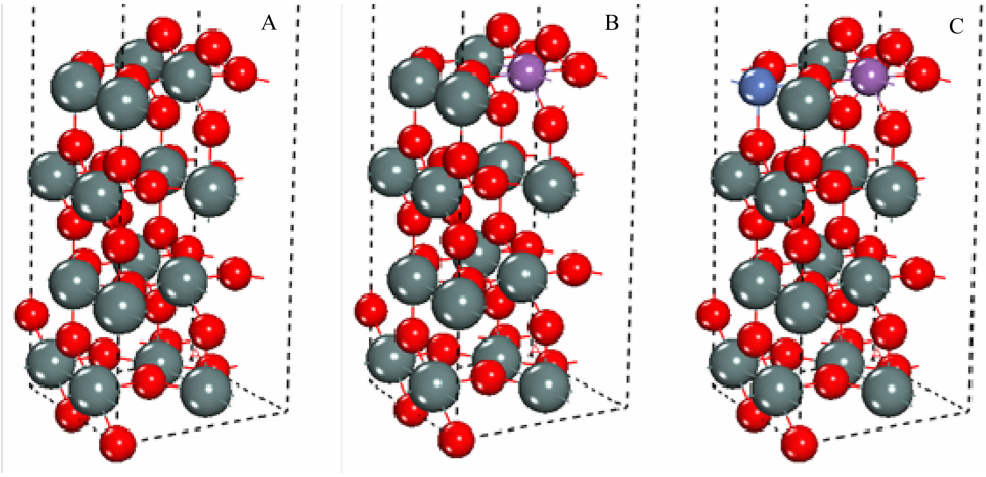

Fig. 1 Models showing the SnO_2(110) facet (A), the preferred site for antimony doping on the top layer Sb-SnO_2 (B) and the preferred site for further nickel doping on the top layer Ni/Sb-SnO_2 (C)[34]. The grey atoms are representative of tin, the purple antimony and the blue nickel.

2.1 Ozone Formation Mechanisms over the β-PbO_2 Catalyst

2.1.1 Determining the Most Stable Surface Facet of the β-PbO_2

Depending on the crystal structure, a surface arrangement can possess an endless number of facets. These can be categorized as either low-index or high-index facet. For this study low-index facets are preferred as they exhibit atomic smoothness. As no previous studies detail the most stable facet, the 100, 110, 111 and 211 facets were all tested. After geometry optimization of each facet, the 110 derivative was deemed the most stable (Figure 2).

When looking at Figure 2 more closely, it can be seen that the arrangement is analogous to that of rutile TiO_2 and SnO_2, both well-known metal oxides and therefore the high stability of this (110) derivative is expected.

2.1.2 Surface Oxidant Formation and the Construction of a Phase Diagram

It is expected that when carrying out the reaction experimentally the surface of a catalyst will undergo some degrees of oxidation. Structu rally, the model shows the surface (or top layer) with four active sites, or four lead atoms with the potential to be oxidized. From Figure 2 it can be seen that two lead atoms reside on the top-sites and two on the bridging sites. As the level of oxidation was not known, the partial coverage and full coverage of the surface were tested. This corresponds to coverages of 0.25, 0.5, 0.75 and 1 mono-layer (ML).

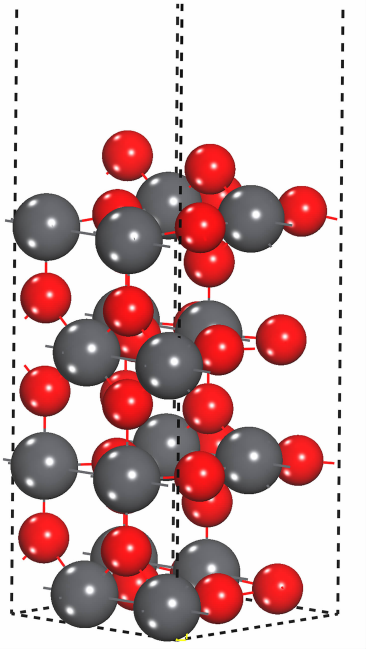

Fig. 2 Model showing the structure of optimized β-PbO_2(110). The grey atoms represent lead and the red atoms represent oxygen.

The EOP mechanism shows that the overall oxidation process is the splitting of H_2O forming O_3. This coupled with the exposure to the atmosphere would result in OH and O being the main surface oxidants. As well as OH and O, the possibility of surface H^+ must also be accounted for as a proton was lost in Steps 1 and 2 (Reactions R7 and R8 as shown above).

When performing geometry optimization calculations using DFT, the resulting energy is termed the total energy of the system. When constructing a phase diagram the free energy is required. This was calculated using Equation 2:

$$\Delta G = \Delta E + \mathrm{ZPE} - T\Delta S \qquad \text{(E2)}$$

where ΔE is the total energy of the system, the most stable optimized surface; ZPE is the zero-point energy, or the ground state energy; and $T\Delta S$ is the temperature times the entropy of the system. Although studies have been carried out in both acidic and basic conditions, acidic conditions were favoured and so a pH correction factor was also considered.

After calculating the most stable surface arrangement for all coverages the free energies were calculated and a phase diagram was constructed (Figure 3). Considering the levels of oxidation studied, it was found that 0.5 ML coverage of OH_{ads}/O_{ads} was closest to that of the experimental potential applied (~1. 9 V vs. SHE) and thus preferred.

2.1.3 Mechanistic Studies Showing the Formation of O_3

The mechanism proposed by Foller and various other groups shows the formation of O_3 via a series of water spitting reactions (R7 to R10 as shown above), where O_2 was formed prior to the formation of O_3. This research investigates each of these four steps in dividually with the main emphasis being on Steps 3

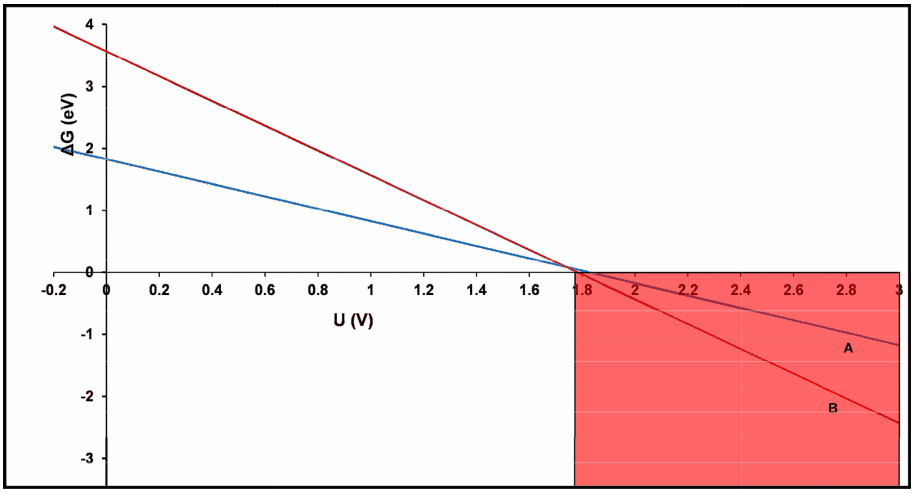

Fig. 3 Plot of ΔG of formation of surface oxidants (OH and O) against applied potential (vs. SHE) on the β-PbO_2 (110) surface. The blue line (Line A) represents the stability of adsorbed OH with potential and the red line (Line B) represents the stability of adsorbed O with potential. The white area represents the potential region in which no surface oxidants are present and the red area represents the potential region where the adsorbed OH and O species are formed with O being the predominant surface oxidant.

and 4 (R9 and R10) which are the formations of O_2 and O_3, respectively.

2.1.3.1 Step 1 — The Splitting of H_2O to Form OH

Step 1 involves the adsorption of H_2O onto the PbO_2 surface, which is then deprotonated to OH, H^+ and e.

$$H_2O \rightarrow OH^{\bullet}(ads) + H^+ + e \quad (R7)$$

When carried out experimentally, the applied potential causes the H_2O to split at the anode. The OH is left adsorbed at the anode and the H^+ passes through the Nafion membrane to reach at cathode where it is reduced to H then two H combine forming H_2.

2.1.3.2 Step 2 — The deprotonation of OH to form O

In Step 2 the OH adsorbed from Step 1 is deprotonated further to form O and release H^+ and electron.

$$H^{\bullet}(ads) \rightarrow O^{\bullet}(ads) + H^+ + e \quad (R8)$$

Again by applying a potential, all OH would be deprotonated further to form O. As discussed in the above section 2.1.2, the optimal coverage was found to be 0.5 ML. This would involve the adsorption of 0.5 ML of OH, which is taken from the adsorption of two H_2O molecules from Step 1 over the unit cell. By deprotonating both the adsorbed OH species, the resulting two O atoms would be ready for Steps 3 and 4, whilst two H^+ would diffuse to cathode where they would be reduced to form H_2 like in the step 1.

2.1.3.3 Step 3— Surface O_2 formation via the interaction of surface O

After Steps 1 and 2, the surface has two O atoms adsorbed on the top sites. These interact with bridging O from the original surface, forming O_2(ads), with some of this leaving the surface as O_2 (gas).

$$2O^{\bullet}(ads) \rightarrow O_2(ads) \rightarrow O_2 \quad (R9)$$

In all reactions there would be an initial state (IS), a transition state (TS) and a final state (FS). The IS is deemed the starting point, the TS is the point where the surface adsorbates are highest in energy level and the FS is the product of the reaction. In this case the IS is adsorbed O formed from H_2O in Step 1, the TS is adsorbed O in close proximity to bridging O but before bond formation and the FS is O_2(ads). On finding stable geometries for these three states a reaction profile for Step 3 could be constructed (Figure 4).

2.1.3.3.1 Initial State of Reaction

The IS of the reaction, as mentioned previously, is two O atoms adsorbed on the top site lead atoms. This corresponds to 0.5 ML coverage of O. The bond distance between the top site and bridging O atoms is 0.2199 nm. The most stable arrangement of the IS has a total energy of -258.95 eV. In the IS shown in

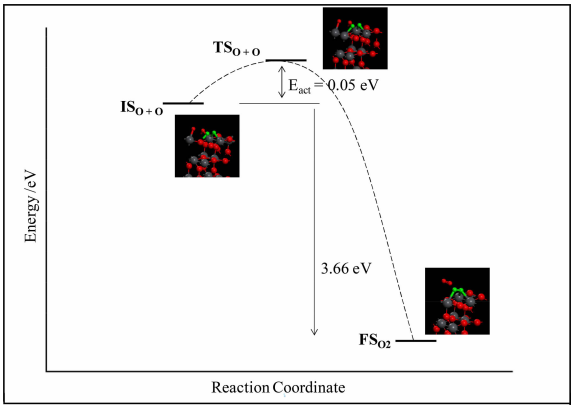

Fig. 4 Energy profile for Step 3 of the mechanism discussed: the formation of surface O_2 from two adsorbed oxygen atoms. The two O atoms highlighted in green are the interacting atoms in the mechanism. The IS shows the adsorbed O and bridging surface O, the TS shows both these two O atoms in a closer proximity to one another, and the FS shows both atoms bonded to form surface O.

Figure 4, the green atoms are the two interacting O atoms.

2.1.3.3.2 Transition State of Reaction

The TS is defined as the point which is highest in energy level. In Step 3, the TS is therefore the point in which the two adjacent O atoms (top site and bridging) are closest without bond formation taking place. Locating the TS can often be the most challenging step of the three. By using computational methods, employing the constrained minimization technique discussed earlier, finding the TS is made easier. After determining the most stable arrangement of an adsorbate(s); in this case the O atom, a frequency calculation is run. The distance between the two interacting atoms is fixed, or constrained, and optimized with respects to all remaining degrees of freedom. The bond distance continually changes with each iteration, until the conditions for the TS have been satisfied.

In finding the TS, the activation energy (E_{act}) can then be calculated:

$$E_{act} = E_{TS} - E_{IS} = (-258.90) - (-258.95) = 0.05 \text{ eV} \quad (E3)$$

The E_{act} was calculated at only 0.05 eV. Thermodynamically the progression from IS to TS would occur with ease. Both the IS and TS are structurally similar, with bond distance the only difference, hence the favourable minor E_{act} barrier to overcome.

2.1.3.3.3 Final State of Reaction

The FS of the reaction shows the formation of O_2(ads). This occurs via the same top site bridging site interaction shown in the IS. From Figure 4 it can be seen that there is both O_2 adsorbed on the surface and O_2 desorbed. Comparing this observation with what is seen in the literature, this O_2(ads)/O_2(gas) type state is in agreement with experimental findings. The overall current efficiency values for O_3 formation on β-PbO_2 struggles to reach 10%[18]. This suggests that for every 100 O_2 molecules formed only 10 will remain adsorbed to the surface. The optimized structure for this FS has a total energy of -262.61 eV.

The enthalpy change (ΔH) associated with the overall reaction can be calculated using Equation 4:

$$\Delta H = E_{FS} - E_{IS} = (-262.61) - (-258.95) = -3.66 \text{ eV} \quad (E4)$$

An enthalpy change of -3.66 eV suggests a FS which is very stable in comparison with the IS. The reaction can also be deemed spontaneous and exothermic. To further investigate the stability, the adsorption energy (E_{ads}) for O_2 can be calculated:

$$E_{ads}(O_2) = E_{(\text{surface } O_2)} - E_{(\text{clean surface})} - E(O_2) = (-252.69) - (-242.77) - (-9.85) = -0.11 \text{ eV} \quad (E5)$$

The adsorption energy was calculated to be-0.11 eV. This suggests a weak adsorption of O_2 to the surface. DFT modelling was carried out in the gas phase, whereas experimentally an acidic aqueous electrolyte is employed[22]. Considering this, the reaction itself can be modelled as a liquid phase also. It is assumed from previous work by Kavanagh et al. that the aqueous electrolyte would have a stabilization effect of around -0.30 eV[49]. If this is added to the adsorption of O_2 in the gas phase, the adsorption energy increases to ~ -0.40 eV, making the adsorption much stronger therefore increasing its stability. This method is employed in Step 4 of the model, with the results shown in the next section. This stabilization effect could be explained by the H_2O/electrolyte solution acting as a cage of hydrogen bonding located above the surface.

These interactions cause the O_2 to remain adsorbed for long enough so that O_3 is formed.

2.1.3.4 Step 4— The Association of Surface O_2 and O to Form O_3

2.1.3.4.1 1st step: The Adsorption of H_2O

In Step 4 the O_2 formed in Step 3 interacts with surface O to form O_3. This O atom is obtained by adsorption of H_2O onto a free lead site adjacent to O_2 (ads).

$$O_2(ads) + O^{\bullet}(ads) \rightarrow O_3(ads) \rightarrow O_3 \quad (R10)$$

The H_2O can be adsorbed on either the top site or bridging region. After calculations the bridging site is deemed more stable; with the $E_{ads}(H_2O)$ also being calculated using Equation 6:

$$E_{ads}(H_2O) = E_{(surface\ H_2O)} - E_{(clean\ surface)} - E_{(H_2O)} = (-326.49)-(-311.69)-(-14.22) = -0.59\ eV \quad (E6)$$

2.1.3.4.2 2nd step — The Deprotonation of H_2O to OH and O

After finding a stable arrangement of H_2O on the surface, the 2nd step in the formation of surface O can occur. To do this the H_2O must undergo a double deprotonation. The best way to do this is to carry out each of the deprotonations individually, e.g. deprotonate to OH first, and then to O. After the most stable OH arrangement has been determined, a second deprotonation to O can occur. Each of these deprotonations will have a Gibbs free energy (ΔG_{rxn}) determined by using Equation 7 below:

$$\Delta G_{rxn} = G(OH) + G(H^+ + e) - G(H_2O) = (-321.29) + (-3.44) - (-325.90) = 1.17\ eV \quad (E7)$$

According to the calculated ΔG_{rxn}, a minimum potential of 1.17 V would be required for this deprotonation to occur[50]. This is in agreement with the experimental onset which is around 1.80 V or above depending on the relevant conditions.

The second deprotonation will quickly follow as the OH is further deprotonated to surface O. Again the Gibbs free energy (ΔG_{rxn}) was calculated using Equation 7 shown above:

$$= (-316.20) + (-3.44) - (-321.29) = 1.65\ eV \quad (E8)$$

The ΔG_{rxn} for this deprotonation was calculated at 1.65 eV. This suggests that a minimum potential of 1.65 V is required for the second deprotonation to take place. Again this is below the experimental onset of 1.8 V. It should be noted that the second deprotonation requires a higher potential than the first. As a result the second deprotonation is more difficult than the first. This is because that after the first deprotonation, the adsorbate would have changed and as such the potential would change.

2.1.3.4.3 The Formation of O_3 via O and O_2 Coupling

Like Step 3, Step 4 would have IS, TS and FS. The IS is O_2(ads) and O(ads), the TS shows O_2(ads) and O(ads) in close proximity with one another but before bonding formation, and the FS is O_3(ads).

2.1.3.4.3.1 Initial State of Reaction

The IS of the reaction involves O_2(ads) and O(ads). The bond distance between these two is 0.334 nm. The most stable geometry of this IS has a total energy of -316.22 eV.

2.1.3.4.3.2 Transition State of the Reaction

In Step 4, the TS is the point in which the O_2 and O are closest without bond formation taking place. After satisfying the parameters required to determine a suitable TS, the activation energy (E_{act}) can be calculated:

$$E_{act} = E_{TS} - E_{IS} = (-315.81) - (-316.22) = 0.41\ eV \quad (E9)$$

The barrier of 0.41 eV suggests that the reaction would precede favourably at room temperature. Considering the value for O_2 adsorption calculated earlier (Eq. 5), it is assumed that this large difference in energy would prevent the reaction with surface O shown in Step 4. The water stabilization effect discussed previously results in the adsorption of O_2 becoming more substantial (~ -0.40 eV), thus, increasing the time for surface O_2 to react with surface O before desorption. The current efficiency (~ 10%) for this system is low, therefore only a small portion of O_2 will stay adsorbed long enough to react and form O_3.

2.1.3.4.3.3 Final State of the Reaction

The FS of the reaction involves the formation of O_3(ads). This occurs through the coupling of O_2 and O. The enthalpy between the IS and FS can be calculated using Equation 10:

$$\Delta H = E_{FS} - E_{IS} = (-316.29) - (-316.22) = -0.07\ eV \quad (E10)$$

The ΔH change was found to be quite small, -0.07 eV, suggesting a slightly favoured FS (Figure 5). This small difference in energies agrees with the thermodynamics, as O_2 is thermodynamically more stable than O_3, meaning that the reverse process can occur leading to the decomposition to O_2.

The $E_{ads}(O_3)$ was then calculated to determine the strength of adsorption and thus the stability of the O_3 molecule:

$$E_{ads}(O_3)=E_{(surface\ O_3)}- E_{(clean\ surf.)} - E(O_3) = (-316.29)-(-301.55) - (-13.50)= -1.24\ eV \quad (E11)$$

The value of -1.24 eV suggests a rather strong adsorption to the surface, and so it is likely that the significant amount of surface ozone may not desorb to electrolyte solution then gas phase, but instead may undergo dissociation/decomposition back to O_2.

When looking more closely at Figure 5, it can be seen that the formation of O_3 occurs on the surface through an Eley-Rideal type mechanism in which the O_2 formed on the surface from Step 3 would desorb and then attack surface O forming O_3 adsorbed on the surface.

2.2 Ozone Formation over the Ni/Sb-SnO_2 Catalyst

With regards to the Ni/Sb-SnO_2, the same four water splitting reaction steps were employed as seen in above section 2.1 on β-PbO_2. Therefore the calculating of a stable surface facet, the surface phase diagram and the water splitting mechanism for Ni/Sb-SnO_2 catalyst are all discussed in this section. There is conflict in the literature with regards to the water splitting mechanism discussed previously for β-PbO_2. The majority of literature reports suggest that the formation of O_3 would occur through O_2H and O_3H intermediates as opposed to direct O_3 formation. This section will discuss both in detail with a greater emphasis on their direct formation of O_3 as opposed to the intermediate states.

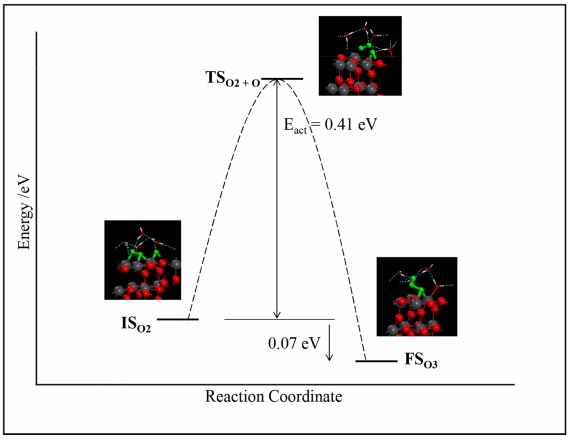

Fig. 5 Energy profile for Step 4 of the mechanism discussed: the transformation from O_2 and O to O_3. The O atoms highlighted in green are the interacting atoms in the mechanism. The IS shows surface O_2 and O, the TS shows the O_2 desorbed with O still adsorbed, and the FS shows O_3 adsorbed on the surface.

2.2.1 Most Stable Surface Facet

In agreement with the study reported by Batzill et al.[44], the SnO_2(110) facet was calculated to be the most stable one and thus the doping with Sb and Ni was carried out on this facet (Figure 6A). Batzill et al. also discussed the possibility of surface vacancies or defects, where it was suggested that the SnO_2 was especially susceptible to the presence of an oxygen vacancy (Figure 6B). By creating this vacancy, two cationic Sn sites form which act as Lewis acidic sites and consequently this site tends to be particularly reactive.

Figure 6A shows the most stable arrangement of Ni/Sb-SnO_2(110), with Sb occupying the bridged region and Ni occupying the top site region. The oxygen vacancy was modelled at different oxygen sites and it was found that the preferred vacancy was the bridged oxygen close to the Sb as shown in Figure 6B.

2.2.2 Construction of Phase Diagram for Ni/Sb-SnO_2

Using the same method shown in section 2.1, a phase diagram (Figure 7) could be constructed for Ni/Sb-SnO_2. Again the geometry optimization yielded a total energy which was inputted into equation 2 yielding the free energy which in turn could be used to plot a phase diagram. It can be seen clearly from the Figure 7 that adsorbed OH could be formed at potentials above 1.57 V (vs. SHE) and would be the dominant oxidant species whilst O could be formed at potentials above 1.92 V.

After determining the free energies for OH and

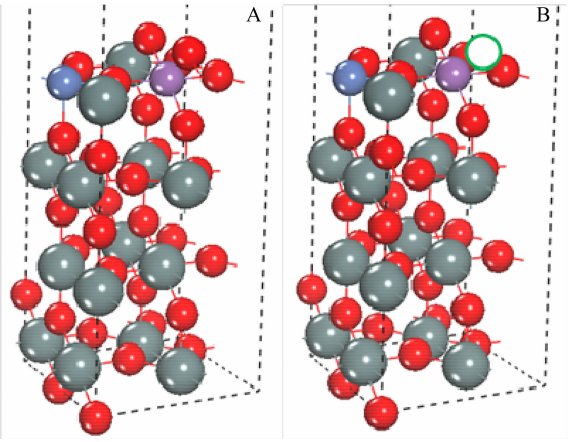

Fig. 6 Models showing the SnO_2 (110) facet doped with Ni and Sb (A) and the same surface but with an oxygen vacancy (B).The grey atoms are Sn, the purple is Sb, the blue is Ni and the green circle represents the vacant site[34].

O, at the selected sub- and mono-layer (ML) coverages, phase diagrams can be constructed. Considering the levels of oxidation studied, it was found that similar to β-PbO_2, the 0.5 ML coverage was the optimum one as it was formed within the experimental applied potential window for the Ni/Sb-SnO_2 system (~ 2.7 V).

2.2.3 Mechanistic Studies of O_3 Formation over Ni/Sb-SnO_2(110)

Steps 1 and 2 (reactions R7 and R8) have already been detailed above in section 2.1.3, and as shown in the phase diagram (Fig. 7) these would occur with ease after a potential (above 1.57 V vs. SHE for step 1 and 1.92 V for step 2) being applied across the surface of anode, therefore the main focus of this section will be the steps 3 and 4, the formation of O_2 and O_3.

2.2.3.1 Step 3 — The Formation of O_2

The literature reports conflicted theories on how step 3 could occur. It has been suggested that the formation of O_2 could occur via the direct interaction of two O atoms, whereas various groups studying the Ni/Sb-SnO_2 system suggest O_2 formation through the formation of an O_2H intermediate. These conflicting reactions could be seen below:

$$2O^{\bullet} \rightarrow O_2(ads) \rightarrow O_2(gas) \quad (R11)$$

$$2OH^{\bullet} \rightarrow O_2 + 2H^+ + e \quad (R12)$$

Both of these pathways were tested to determine which pathway would be favored. Upon determining the IS, TS and FS of each pathway, energy profiles for all pathways studied were constructed and compared to determine which pathway would be preferred thermodynamically. Reactions 11 and 12 are discussed in two separate sections (2.2.3.2 and 2.2.3. 3).

2.2.3.2 The Formation of O_2 via an O_2H Intermediate

In this section, the formation of O_2 is discussed as going through an OH intermediate as opposed to the direct combination of two O atoms discussed in the next section (2.2.3.3). After H_2O would has

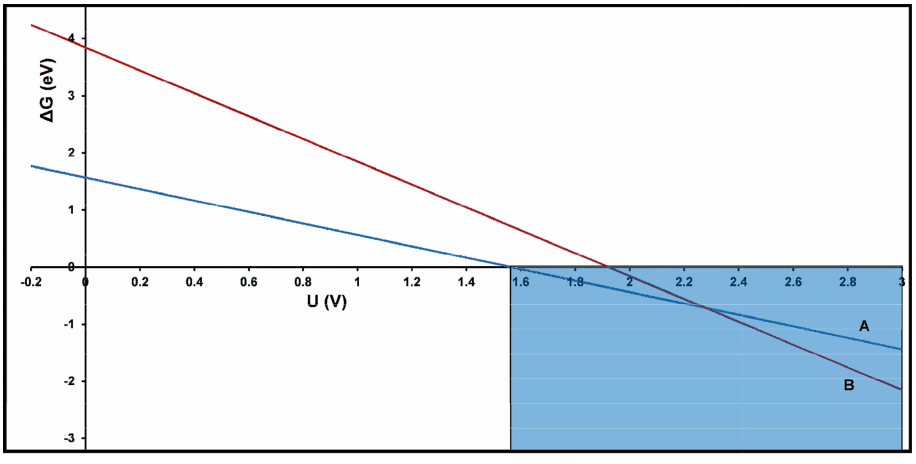

Fig. 7 Plot of ΔG of formation of surface oxidants against applied potential (vs. SHE) on the Ni/Sb-SnO_2 surface. The blue line (line A) represents the stability of adsorbed OH with potential and the red line (line B) represents the stability of adsorbed O with potential. The white area represents the potential region in which no surface oxidants are present and the blue area represents the potential region where OH and O could be formed with the OH being the predominant surface oxidant at above 1.57 V.

adsorbed onto the surface and been deprotonated to OH, rather than undergoing further deprotonation, it would interact with O from the surface yielding O_2H as an intermediate.

The IS of reaction would be adsorbed OH and O, the TS would be where the OH and O being closest before bond formation taking place, the Intermediate (IM) would be the formation of O_2H and the FS would be the formation of O_2(ads).

2.2.3.2.1 Initial State of Intermediate

The IS in the formation of O_2H would be OH adsorbed on the top site region and an O atom adsorbed in the surface vacancy reforming the O bridge. The optimized bond distance between the two interacting O and OH was 0.340 nm with a total energy of -301.16 eV.

2.2.3.2.2 Transition State of Intermediate

The geometry of the TS was similar to that of the IS, with the OH and O being adsorbed on the surface (Figure 8). The TS was deemed the highest point in energy between the two adsorbates before bond formation occurring. After finding the TS, the activation energy could be calculated using Equation 12:

$$E_{act} = E_{TS} - E_{IS} = (-300.16) - (-301.17) = 1.01 \text{ eV} \quad \text{(E12)}$$

The E_{act} was calculated to be 1. 01 eV. In terms of the thermodynamics, the progression from IS to TS would occur slowly, as the higher the barrier is the slower the reaction will occur.

2.2.3.2.3 Final State of Intermediate

The FS is the formation of O_2H in which surface OH and O from the IS interact with each other. The energy associated with this FS was -300.75 eV with the enthalpy calculated using Equation 13:

$$\Delta H = E_{FS} - E_{IS} = (-300.75) - (-301.17) = 0.42 \text{ eV} \quad \text{(E13)}$$

This enthalpy change of 0.42 eV suggests an endothermic reaction. Figure 8 shows that the FS would be less stable than the IS. In order to be more stable the FS should be lower in energy than the IS. The arrangement of the IS is OH and O, whereas the FS is O_2H. By comparing both states, the positive change in enthalpy is not surprising, as the IS being made up of OH and O which are well known intermediates that

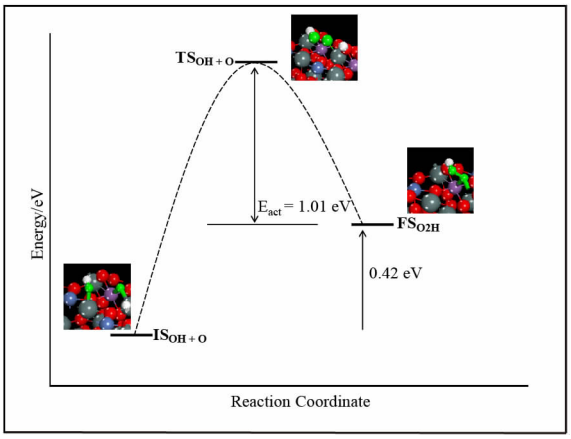

Fig. 8 Energy profile for Step 3 of the mechanism discussed: the formation of an O_2H intermediate from OH (ads) and O(ads). The O atoms highlighted in green are the interacting atoms in the mechanism. The IS shows the adsorbed OH and O, the TS shows both these atoms in a closer proximity to one another, and the FS shows both atoms bonded to form an O_2H intermediate.

are relatively more stable than the O_2H considered in the FS, the latter would be expected to be less stable in comparison.

2. 2. 3. 2. 4 The Deprotonation of O_2H

After the formation of the O_2H intermediate discussed previously in the above section, the final step of the reaction would be the deprotonation to form O_2. The difference in energy between these was calculated, and in fact it was simply the energy required to remove a proton from the adsorbate. The energy for the O_2H as mentioned previously was -300.75 eV and the energy for O_2 was calculated to be -295.48 eV. This gives an energy difference of 5.27 eV which is considered quite large. Upon deprotonating, the adsorption energy (E_{ads}) for O_2 (ads) can be determined:

$$E_{ads}(O_2) = E_{(\text{surface } O_2)} - E_{(\text{clean surface})} - E(O_2) =$$
$$(-295.59) - (-284.96) - (-9.85) = -0.78 \text{ eV} \quad \text{(E14)}$$

The E_{ads} was calculated at -0.78 eV. This shows a strong interaction between the surface and the adsorbate, resulting in a stable O_2 adsorbate. After calculating the reaction step shown in Equation 12, a comparison with the direct formation of O_2 was calculated, and is discussed in the next section.

2.2.3.3 Direct Formation of O_2 via the Interaction of Two O Atoms

In this case the IS would be two surface adsorbed O atoms, the TS would be the two adsorbed O atoms in closer proximity to one another before bond formation, and the FS would be O_2(ads). After calculating stable configurations for each of these three states, an energy profile was constructed (Figure 9).

2.2.3.3.1 Initial State of Reaction

The IS of reaction was two O atoms adsorbed, with one on the top site and the other on the oxygen vacancy site. The bond distance between these two atoms was 0.338 nm. The most stable arrangement had a total energy of -295. 01 eV.

2.2.3.3.2 Transition State of Reaction

The TS of reaction involved the two O atoms from the IS getting closer in energy to one another before bond formation. The progression from IS to TS was deemed the activation energy (E_{act}) and was calculated below:

$$E_{act} = E_{TS} - E_{IS} = (-294.67) - (-295.01) = 0.34 \text{ eV} \quad \text{(E15)}$$

The E_{act} calculated was only 0.34 eV. Thermodynamically the progression from IS to TS should occur with ease. When considering the high potential (2.7 V) used experimentally, this shows further agreement that the reaction would proceed easily.

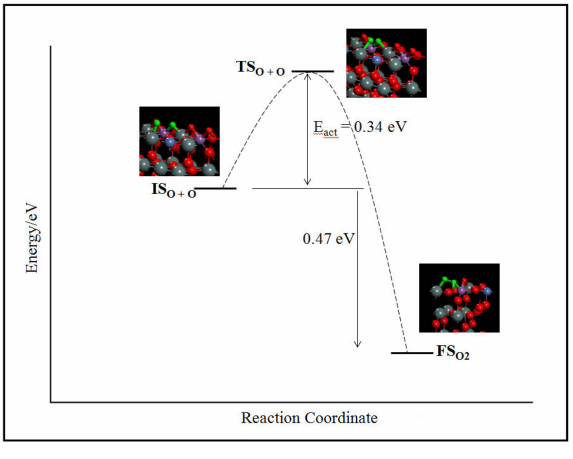

Fig. 9 Energy profile for Step 3 of the mechanism discussed: the formation of surface O_2 from two adsorbed oxygen atoms. The O atoms highlighted in green are the interacting atoms in the mechanism. The IS shows the adsorbed O and bridging surface O, the TS shows both these atoms in a closer proximity to one another, and the FS shows both atoms bonded to form surface O_2[34].

2.2.3.3.3 Final State of Reaction

The FS of the reaction was the formation of O_2(ads). This occurred via the interaction of the top site and bridging O atoms from the IS. The geometry or surface arrangement of this O_2 was of particular interest in this step. The different O_2 arrangements tested are shown in Table 1:

Out of these five common surface arrangements, only the bridging and end-on arrangements were deemed suitable as possible FS's for Step 3 as the rest would have desorbed.

Tab. 1 Possible O_2 arrangements and their associated energies

O_2 arrangement	Energy/eV
Bridging	-295.48
Top site	Desorbed
End-on	-295.60
Disigma	Desorbed
Griffiths	Desorbed

The enthalpy for each of these can be calculated using Equation 16, with the data being presented in Table 2:

Tab. 2 The enthalpy changes in both the bridging and end-on geometries

O_2 arrangement	Enthalpy change(ΔH)/eV
Bridging	-0.47
End-on	-0.60

$$\Delta H = E_{FS} - E_{IS} \quad \text{(E16)}$$

Table 2 shows that the end-on arrangement was more stable than the bridging analogue, it is, therefore, important to address why the bridging analogue was used. In Step 4, after coupling these two arrangements with surface O/OH, it was found that the formation of O_3 would only occur through the interac-

tion of bridging O_2 with surface O/OH. In the case of end-on, O_3 formation does not occur, highlighting that these catalysts could be selective.

An enthalpy of -0. 47 eV for bridging O_2 corresponds to a FS that is more stable in comparison to the IS. The reaction could be deemed spontaneous and exothermic. As O_2 is a stable molecule, the E_{ads} (O_2) can also be calculated:

$$E_{ads}(O_2) = E_{(surface\ O_2)} - E_{(clean\ surface)} - E(O_2) = (-295.48) - (-284.96) - (-9.85) = -0.68\ eV \quad (E17)$$

The adsorption energy was calculated at -0. 68 eV. This suggests a significant interaction with the surface, further highlighting the stability of O_2. As the E_{act} is in fact lower than the adsorption of O_2 (essentially the activation energy for O_2 desorption), the O_2 could remain adsorbed long enough to interact with O(ads) in Step 4 (see below).

2. 2. 3. 4 Step 4 — Comparing Pathways for the Formation of O_3

It is in Step 4 where again like Step 3 the formation of O_3 could occur through either an OH intermediate or an O atom as shown in Reactions 13 and 14:

$$O_2 + O^{\bullet} \rightarrow O_3 \quad (R13)$$

$$OH^{\bullet} + O_2 \rightarrow O_3H \rightarrow O_3 \quad (R14)$$

Step 4, the formation of O_3 is the most difficult step in the reaction series. O_2 is thermodynamically more stable than O_3 and the reaction must have a high overpotential for O_2 formation to overcome this thermodynamic barrier. Both Reactions 13 and 14 show different pathways in the formation of O_3. Section 2.2.3.5 will focus on explaining the results found for Reaction 13 and Section 2.2.3.6 highlights the results found for Reaction 14.

2.2.3.5 The Direct Formation of O_3 via the Coupling of O_2 and O

2.2.3.5.1 Step 1— The Adsorption of OH

In Step 4, O_2 interacts with O(ads) to form O_3 (Reaction R13). The O is sourced from the adsorption of OH (from electrolyte) and its deprotonation to O.

This OH could be adsorbed on either the top site or bridging region. Upon calculation of both, it was found that the OH preferred to arrange on the top site with a total energy of -304.99 eV as opposed to -304.80 eV when bridged.

2.2.3.5.2 Step 2— The Deprotonation of OH to Form O

After successful adsorption of OH to the surface, the OH must undergo deprotonation to form surface O. With each deprotonation there was a Gibbs free energy (ΔG_{rxn}) that could be calculated. This was used to determine the minimum applied potential required for the deprotonation to occur:

$$\Delta G_{rxn} = G(O) + G(H^+ + e) - G(OH) = (-299.18) + (-3.44) - (-304.58) = 1.96\ eV \quad (E18)$$

Equation 18 shows the Gibbs free energy calculated for the deprotonation of OH being 1.96 eV. This suggests that a minimum applied potential of 1.96 V would be required for the second deprotonation to take place. This seems slightly higher than the experimental onset potential, but still well within the electrochemical window of study (2.7 V) for Ni/Sb-SnO_2.

2.2.3.5.3 Step 3— The Reaction of O_2 (ads) and O (ads) Forming O_3(ads)

The IS is O_2(ads) and O(ads), the TS is the point in which O_2(ads) and O(ads) is highest in energy level before bond formation taking place and the FS is O_3 (ads).

2.2.3.5.3.1 Initial State of Reaction

The IS of the reaction is O_2 (ads) and O (ads). The optimized bond distance between these two is 0.335 nm and the total energy of the system is -299.29 eV.

2.2.3.5.3.2 Transition State of Reaction

In this step, the TS would be similar to the IS with O_2 and O both still adsorbed to the surface, with a state that was lower in energy than the IS whilst not being bonded. After calculating a stable geometry for TS the activation energy from IS to TS can be calculated:

$$E_{act} = E_{TS} - E_{IS} = (-298.52) - (-299.29) = 0.77\ eV \quad (E19)$$

Equation 19 shows that the E_{act} was calculated to be 0.77 eV. This suggests that the reaction would be slow at room temperature, as the higher the E_{act} the slower the reaction. Taking into consideration that the experimentally applied potential was 2.7 V, this

should drive the reaction to completion. Experimentally, this reaction was run in aqueous electrolyte, therefore, the water stabilization effect discussed by Kavanagh et al. [49] would lower this barrier further. It should be noted that the activation barrier for gas phase O_3 formation was only slightly higher than the adsorption energy in Step 3 (the energy for desorption of O_2), if taking the high applied potential and the water stabilizing effect, the barrier would be considerably lower if modelled as a liquid phase reaction, suggesting a feasible process to occur at room temperature.

2.2.3.5.3.3 Final State of Reaction

The FS of Step 4 involves the formation of O_3(ads). This takes place through the coupling of O_2 and O (reaction R13). The enthalpy of reaction from IS to FS can be calculated using equation 20:

$$\Delta H = E_{FS} - E_{IS} = (-299.34) - (-299.29) = -0.05 \text{ eV} \quad \text{(E20)}$$

The enthalpy change was only at -0.05 eV, suggesting a slightly more favorable FS (Figure 10). This is not surprising as, O_2 is thermodynamically more stable than O_3, and therefore the O_3 is likely to decompose back to O_2 and O via the reverse process. This is why a high overpotential is required experimentally for O_3 formation. Through this high overpotential, the O_2 sites would be inhibited and hence promote O_3 formation, therefore stopping this decomposition.

In addition to the ΔH, the $E_{ads}(O_3)$ can be calculated to determine its stability on the surface. This was achieved by measuring the strength of adsorption of O_3 to the surface:

$$E_{ads}(O_3) = E_{(\text{surface } O_3)} - E_{(\text{clean surface})} - E(O_3) = (-299.34) - (-284.96) - (-13.50) = -0.88 \text{ eV} \quad \text{(E21)}$$

An $E_{ads}(O_3)$ value of -0.88 eV suggests a strong adsorption to the surface and consequently stable adsorption on the surface. However, if the coverage and entropy changes for the adsorption were considered, the value would be reduced to around -0.15 eV at the standard states[34], yielding a much weaker adsorption to the surface.

When looking more closely at Figure 10, it can be seen that the surface mechanism for O_3 formation

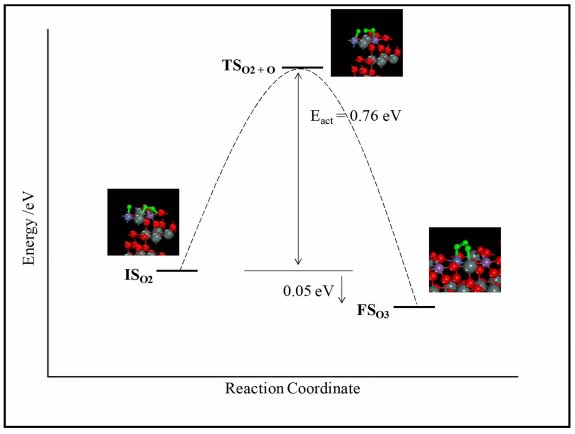

Fig. 10 Energy profile for Step 4 of the mechanism discussed: the transformation from O_2 and O to O_3. The O atoms highlighted in green are the interacting atoms in the mechanism.The IS shows the O_2 (ads) and O (ads), the TS shows both these atoms in a closer proximity to one another, and the FS shows both atoms bonded to form surface O_3[34].

occurs through a Langmuir-Hinshelwood interaction in which both O_2 and O are surface adsorbed species. These adsorbed species interact with each other forming O_3 on the surface before desorbing as gaseous O_3.

2.2.3.6 The Formation of O_3 via an O_3H Intermediate

In this mechanistic step an O_3H intermediate would be formed before deprotonating to produce O_3. The rationale for calculating this was to determine whether or not the point at which deprotonation occurs has an effect on the reaction kinetics through calculating the activation barrier of this O_3H intermediate. Through the adsorption of OH, as discussedin Section 2.2.3.5.1, the surface adsorbates present were O_2(ads) and OH(ads). Previously, this OH was further deprotonated to O(ads), however, in this case direct interaction of O_2 and OH were tested without deprotonation.

2.2.3.6.1 The Interaction of O_2(ads) and OH(ads) Forming an O_3H Intermediate

This pathway involves the interaction of O_2(ads) from Step 3 and OH generated from adsorbed H_2O. The previously discussed pathway shows the direct formation of O_3 through the deprotonation of OH and subsequent interaction with O_2 forming O_3. In this

section an attempt was made at carrying out the deprotonation after the interaction of O_2 and OH to form an O_3H intermediate.

Upon calculation it was found that in each instance the O_3H dissociated back to OH and O_2, suggesting that these adsorbates possess a greater stability when compared with O_3H. Due to the instability of the O_3H intermediate and the unlikelihood that the re action would precede via this pathway, no further calculations were carried out. The feasibility of an O_3H intermediate should be considered by including some experimental parameters (temperature, electrolyte flow rate, potential). However, as these calculations proved extensive and beyond the scope of this paper, they were no longer looked at in detail with regards to this study and further results will be discussed in future publications.

2.3 Catalyst Activity, Selectivity, Lifetime and Regeneration

To develop an efficient catalyst, in addition to high activity and good selectivity, the lifetime must also be considered. For a catalyst to have a long lifetime, it must be able to regenerate itself. This is an area that requires further research with regards to the electrochemical ozone production (EOP) employing the Ni/Sb-SnO_2 anodes which have been found to possess a moderate lifetime. Looking at Equation 21, which shows the $E_{ads}(O_3)$, it can be seen that the calculated value of adsorption energy for O_3 (at lower coverage, before taking account of coverage and entropy effects) was -0. 88 eV, suggesting a strong adsorption to the surface. This is problematic as in order to increase the lifetime, hereby making the anode regenerable, this adsorbed O_3 must be easily displaced from the surface, freeing up the active sites for continuing EOP. When trying to desorb the O_3 using DFT modelling, it was found that the O_3 preferred to readsorb onto the surface, reaffirming its stability. This finding suggests that practically, we may need to increase the mass transport to remove the produced surface ozone, by employing flowing electrolyte or by increasing the flow rate of circulated electrolyte solution. This DFT study does highlight the reaction mechanisms, and gives an insight into the reaction barriers and stability of adsorbed species through the calculation of E_{act} and E_{ads}. However, more specific experimental fact ors such as applied potential and flow rate havenot been examined in details within the scope of this study. Nevertheless, O_2 is thermodynamically more stable than O_3, and therefore, O_3 is likely to decompose back to O_2 and O via the reverse process. This is why a high overpotential (e.g. , $>$2.0 V voltage) is required experimentally for O_3 formation. Through this high overpotential, the O_2 sites would be inhibited and hence O_3 formation would promote, therefore, stopping this decomposition and yielding high O_3 selectivity (current efficiency). Although higher voltages will have a positive effect on the O_3 selectivity, the stability of the catalyst may suffer, as a result, the optimum operation voltage (e.g., 2.7 V) is considered suitable to balance both sides in the applications. It should also be noted that this study considers the gas phase reaction, whereas experimentally an aqueous acidic electrolyte is employed. One final thing to be considered is that this study shows the successful formation of a single O_3 molecule on the Ni/Sb-SnO_2, whereas when run experimentally there may be multiple O_2 and O_3 molecules along with other OH and O intermediates on the surface at the one time. As a result there will be electrostatic repulsion between the competing adsorbates herein weakening the O_3 adsorption and leading to the successful desorption of O_3. Taking all of these into account and the high current efficiency (e.g., 50%) values reported, the optimum Ni/Sb-SnO_2 catalyst can clearly represent one that is regenerable and warrants further work to be done both experimentally and theoretically to discover new methods of increasing the overall lifetime.

3 Conclusions

The electrochemical ozone production (EOP) via water splitting reactions has attracted increasing interests, thanks to the promising potential of ozone as a green oxidant for many useful applications such as advanced oxidation processes for water treatment, with the most efficient catalysts developed experimentally being β-PbO_2 and Ni/Sb-SnO_2. Our initial

DFT calculations on these systems, as a first attempt from a theoretical perspective, provided an insight into the complexity of electrocatalysis involved: the preferred surface facet as a function of its stability have been shown, the expected levels of surface oxidation as demonstrated through the construction of phase diagrams, the activation barriers and adsorption energies for O_2 and O_3 formation revealed that Ni/Sb-SnO_2 catalyst is much more active than β-PbO_2 which explained the experimental results. The final thing of interest was the surface reaction mechanism for the formation of O_3. On the β-PbO_2 catalyst the formation of O_3 occurs through an Eley-Rideal style mechanism whereas for Ni/Sb-SnO_2 the surface reactions occurred through a Langmuir-Hinshelwood style interaction. This again highlights the complexity associated with the EOP mechanism and as to why more detailed fundamental studies need to be carried out theoretically in understanding the electrocatalysis and more general surface electrochemistry at the quantum level.

Acknowledgements

We gratefully acknowledge the Department of Education and Learning (DEL) of Northern Ireland, Northern Ireland Water Limited, Modern Water plc, UK EPSRC and Loughborough University for their supports.

References:

[1] Villegas L G C, Mashhadi N, Chen M, et al. A short review of techniques for phenol removal from wastewater [J]. Current Pollution Reports, 2016, 2(3):157-167.

[2] Suzuki H, Araki S, Yamamoto H. Evaluation of advanced oxidation processes (AOP) using O_3, UV, and TiO_2 for the degradation of phenol in water[J]. Journal of Water Process Engineering, 2015, 7(1): 54-60.

[3] Kovalova L, Siegrist L H, von Gunten U, et al. Elimination of micropollutants during post-treatment of hospital wastewater with powdered activated carbon, ozone, and UV[J]. Environmental Science & Technology, 2013, 47 (14): 7899-7908.

[4] Luyten J, Sniegowski K, Van Eyck K, et al. AOX removal from industrial wastewaters using advanced oxidation processes: Assessment of a combined chemical-biological oxidation[J]. Water Science and Technology, 2013, 68(9): 2048-2054.

[5] Chin A, Bérubé P R. Removal of disinfection by-product precursors with ozone-UV advanced oxidation process[J]. Water Research, 2005, 39(10): 2136-2144.

[6] Iliadis D, Millar B J. Ozone and its use in periodontal treatment[J]. Open Journal of Stomatology, 2013, 3(2): 197-202.

[7] Domb WC. Ozone therapy in dentistry[J]. Interventional Neuroradiology, 2014, 20(5): 632-636.

[8] Sousa C S, Torres L M, Azevedo M P F, et al. Ozônio na esterilização de produtos para assistência à saúde: Revisão integrativa da literatura[J]. Revista da Escola de Enfermagem da USP, 2011, 45: 1243-1249.

[9] Iwamura T, Nagano K, Nogami T, et al. Confirmation of the sterilization effect using a high concentration of ozone gas for the bio-clean room[J]. Biocontrol Science, 2013, 18 (1): 9-20.

[10] Onyango A N. Alternatives to the 'water oxidation pathway' of biological ozone formation[J]. Journal of Chemical Biology, 2016, 8(1): 1-8.

[11] da SilvaL M, Santana M H P, Boodts J F C. Electrochemistry and green chemical processes: Electrochemical ozone production[J] Química Nova, 2003, 26(6): 880-888.

[12] AWW Association. Letterman R D. Water quality and treatment-A handbook of community water supplies, 5th edition[M]. 1999.

[13] Seader J D, Tobias C W. Ozone by electrolysis of sulfuric acid[J]. Industrial & Engineering Chemistry, 2002, 44(9): 2207-2211.

[14] Babak A A, Amadelli R, Fateev V N. Effect of perfluoro compounds on kinetics of the oxygen and ozone formation at the platinum anode[J]. Russian Journal of Electrochemistry, 1998, 34(2): 149-152.

[15] Awad M I, Sata S, Kaneda K, et al. Ozone electrogenera tion at a high current efficiency using a tantalum oxide-platinum composite electrode[J]. Electrochemistry Communications, 2006, 8(8): 1263-1269.

[16] García-Morales M A, Roa-Morales G, Barrera-Díaz C, et al. Synergy of electrochemical oxidation using boron-doped diamond (BDD) electrodes and ozone (O_3) in industrial wastewater treatment[J]. Electrochemistry Communications, 2013, 27(5): 34-37.

[17] Arihara K, Terashima C, Fujishima A. Electrochemical production of high-concentration ozone-water using free standing perforated diamond electrodes[J]. Journal of the Electrochemical Society, 2007, 154(4): E71-E75.

[18] Foller P C, Tobias C W. The anodic evolution of ozone [J]. Journal of the Electrochemical Society, 1982, 129(3): 506-515.

[19] Wang J, Li X, Guo L, et al. Effect of surface morphology of lead dioxide particles on their ozone generating perfor-

mance[J]. Applied Surface Science, 2008, 254(20): 6666-6670.

[20] Basiriparsa J, Abbasi M. High-efficiency ozone generation via electrochemical oxidation of water using Ti anode coated with Ni-Sb-SnO_2[J]. Journal of Solid State Electrochemistry, 2012, 16(3): 1011-1018.

[21] Christensen P A, Imkum A. The inhibition of ozone generation at Ni/Sb-SnO_2 electrodes in high concentrations of dissolved O_3[J]. Ozone: Science & Engineering, 2011, 33(5): 389-395.

[22] Wang Y H, Cheng S A, Chan K Y, et al. Electrolytic generation of ozone on antimony- and nickel-doped tin oxide electrode[J]. Journal of Electrochemical Society, 2005, 152 (11): D197-D200.

[23] Christensen P A, Lin W F, Christensen H, et al. Room temperature, electrochemical generation of ozone with 50% current efficiency in 0. 5M sulfuric acid at cell voltages ＜ 3V[J]. Ozone: Science & Engineering, 2009, 31(4): 287-293.

[24] Christensen P A, Attidekou P S, Egdell R G, et al. Identification of the mechanism of electrocatalytic ozone generation on Ni/Sb-SnO_2 [J]. The Journal of Physical Chemistry C, 2017, 121(2): 1188-1199.

[25] Velichenko A B, Knysh V A, Luk'yanenko T V, et al. Electrodeposition PbO_2-TiO_2 and PbO_2-ZrO_2 and its physicochemical properties[J]. Materials Chemistry and Physics, 2012, 131(3): 686-693.

[26] Yao Y, Zhao M, Zhao C, et al. Preparation and properties of PbO_2-ZrO_2 nanocomposite electrodes by pulse electrodeposition[J]. Electrochimica Acta, 2014, 117: 453-459.

[27] Tan C, Xiang B, Li Y, et al. Preparation and characteristics of a nano-PbO_2 anode for organic wastewater treatment[J]. Chemical Engineering Journal, 2011, 166(1): 15-21.

[28] Velichenko A B, Girenko D V, Kovalyov S V, et al. Lead dioxide electrodeposition and its application: influence of fluoride and iron ions[J]. Journal of Electroanalytical Chemistry, 1998, 454(1/2): 203-208.

[29] Amadelli R, Velichenko A B. Lead dioxide electrodes for high potential anodic processes[J]. Serbian Chemical Society, 2001, 66(11/12): 835-845.

[30] De Sousa L G, Franco D V, Da Silva L M. Electrochemical ozone production using electrolyte-free water for environmental applications[J]. Journal of Environmental Chemical Engineering, 2016, 4(1): 418-427.

[31] Rosestolato D, Amadelli R, Velichenko A B. Electrode characteristics for ozone production: a case study using undoped and doped PbO_2 on porous platinised titanium substrates[J]. Journal of Solid State Electrochemistry, 2016, 20(4): 1181-1190.

[32] Cheng S A, Chan K Y. Electrolytic generation of ozone on an antimony-doped tin dioxide coated electrode [J]. Electrochemical and Solid-State Letters, 2004, 7(3): D4-D6.

[33] Gibson G, Morgan A, Hu P, et al. New insights into electrocatalytic ozone generation via splitting of water over PbO_2 electrode: A DFT study[J]. Chemical Physics Letters, 2016, 654: 46-51.

[34] Gibson G, Wang Z, Hardacre C, et al. Insights into the mechanism of electrochemical ozone production via water splitting on the Ni and Sb doped SnO_2 catalyst [J]. Physical Chemistry Chemical Physics, 2017, 19(5):3800-3806.

[35] Kresse G, Furthmüller J. Efficient iterative schemes for ab initiototal-energy calculations using a plane-wave ba sissset[J]. Physical Review B, 1996, 54(16):11169-11186.

[36] Kresse G, Furthmüller J. Efficiency of ab-initio total energy calculations for metals and semiconductors using a plane-wave basis set[J] Computational Materials Science, 1996, 6(1): 15-50.

[37] Kresse G, Hafner J. Ab initio molecular-dynamics simulation of the liquid-metal-amorphous-semiconductor transition in germanium[J]. Physical Review B, 1994, 49(20): 14251-14269.

[38] Perdew J P, Burke K, Ernzerhof M. Generalized gradient approximation made simple[J]. Physical Review Letters, 1996, 77(18): 3865-3868.

[39] Kresse G, Joubert D. From ultrasoft pseudopotentials to the projector augmented-wave method[J]. Physical Review B, 1999, 59(3): 1758-1775.

[40] Blöchl P E. Projector augmented-wave method[J]. Physical Review B, 1994, 50(24): 17953-17979.

[41] Michaelides A, Liu Z P, Zhang C J, et al. Identification of general linear relationships between activation energies and enthalpy changes for dissociation reactions at sur faces[J]. Journal of the American Chemical Society, 2003, 125(13): 3704-3705.

[42] Liu Z P, Hu P. General rules for predicting where a catalytic reaction should occur on metal surfaces: A density functional theory study of C-H and C-O bond breaking/making on flat, stepped, and kinked metal surfaces[J]. Journal of the American Chemical Society, 2003, 125(7): 1958-1967.

[43] Alavia A, Hu P, Deutsch T, et al. CO oxidation on Pt(111): An Ab initio density functional theory study[J]. Physical Review Letters, 1998, 80(16): 3650-3653.

[44] Batzill M, Diebold U. The surface and materials science

of tin oxide[J]. Progress in Surface Science, 2005, 79 (2/4): 47-154.

[45] Amadelli R, Armelao L, Velichenko A B, et al. Oxygen and ozone evolution at fluoride modified lead dioxide electrodes[J]. Electrochimica Acta, 1999, 45(4/5): 713-720.

[46] Franco D V, Silva L M D, Jardim W F, et al. Influence of the electrolyte composition on the kinetics of the oxygen evolution reaction and ozone production processes[J]. Journal of the Brazilian Chemical Society, 2006, 17(4): 446-757.

[47] Amadelli R, De Battisti A, Girenko D V, et al. Electrochemical oxidation of trans-3,4-dihydroxycinnamic acid at PbO_2 electrodes: direct electrolysis and ozone mediated reactions compared[J]. Electrochimica Acta, 2000, 46(2/3): 341-347.

[48] Amadelli R, Samiolo L, Battisti A D, et al. Electro-oxidation of some phenolic compounds by electrogenerated O_3 and by direct electrolysis at PbO_2 anodes[J]. Journal of the Electrochemical Society, 2011, 158(158): P87-P92.

[49] Kavanagh R, Cao X M, Lin W F, et al. Origin of low CO_2 selectivity on platinum in the direct ethanol fuel cell[J]. Angewandte Chemie International Edition, 2012, 51(7): 1572-1575.

[50] Lin W F, Sun S G, Tian Z Q, et al. Quantum chemistry and *in situ* FTIR spectroscopy studies on potential-dependent properties of CO adsorbed on Pt electrodes[J]. Electrochimica Acta, 1993, 38(8): 1107-1114.

绿色电化学水分解法制备臭氧:机理研究

Gregory Gibson[1,2], 林文锋[1*]

(1. 英国拉夫堡大学化学工程系, 拉夫堡, 莱斯特, LE11 3TU;
2. 英国贝尔法斯特女王大学化学与化学工程学院, 贝尔法斯特, BT9 5AG)

摘要: 采用电催化剂通过水分解反应形成臭氧的绿色节能方法为常规耗能量大的冷电晕放电提供了非常具有吸引力的替代方法. 在大量研究的用于电化学合成臭氧的电催化剂中, β- 氧化铅(β-PbO_2)和氧化锡(SnO_2)基催化剂在室温下最有效.本工作通过密度泛函理论计算,研究了上述两种催化剂作用下臭氧的形成机制. 两种催化剂 β-PbO_2 和镍/锑掺杂氧化锡(Ni/Sb-SnO_2)的(110)晶面最稳定,故作者特别关注 β-PbO_2(110)和 Ni/Sb-SnO_2(110)表面发生的最后两步反应,即氧气和臭氧的形成,模拟了可能的水分解机理. 结果表明,在 β-PbO_2 催化剂的作用下,臭氧是遵循 Eley-Rideal 机理形成,与在 Ni/Sb-SnO_2,表面臭氧的形成机理相反,后者是通过 Langmuir-Hinshelwood 机理形成. 将 β-PbO_2 主要模拟为固-液相,Ni/Sb-SnO_2 主要模拟为气相,计算得到吸附能(E_{ads})、吉布斯自由能(ΔG)和活化能(E_{act})等热力学参数值,并进行了分析与比较. 这些结果为设计和研发新型的高电流效率电化学制臭氧用催化剂提供了依据.

关键词: 臭氧析出反应;水分解;密度泛函理论;电催化;表面吸附和反应;氧化铅;镍/锑掺杂氧化锡